RSC Advances

RSC Publishing

PAPER

View Article Online
View Journal | View Issue

Cite this: *RSC Advances*, 2013, **3**, 8967

Photoswitchable aggregation-induced emission of a dithienylethene–tetraphenylethene conjugate for optical memory and super-resolution imaging†

Chong Li,‡[ab] Wen-Liang Gong,‡[ab] Zhe Hu,‡[ac] Matthew P. Aldred,‡[a] Guo-Feng Zhang,[ab] Tao Chen,[ab] Zhen-Li Huang*[ac] and Ming-Qiang Zhu*[ab]

Received 7th February 2013,
Accepted 28th March 2013

DOI: 10.1039/c3ra40674a

www.rsc.org/advances

We report the synthesis of a dithienylethene–tetraphenylethene (DTE–TPE) conjugated photochromic fluorophore which simultaneously exhibits aggregation-induced emission and reversible fluorescence switching. Photochromic DTE–TPE turns cyan-blue after 5 s of UV irradiation and exhibits a strong green emission at 520–540 nm upon excitation with visible light when present in nanoparticles and the solid state, in contrast to non-fluorescence in solution. DTE–TPE exhibits reversible fluorescence switching under alternating irradiation with UV and visible light (wavelengths greater than 440 nm), when present in nanoparticles and the solid state. The continuous readout of the emissive DTE–TPE film over 1 h upon 440 nm excitation–irradiation causes only a 7% reduction in emission intensity for DTE–TPE. The super-resolution fluorescence nanolocalization indicates that the vicinal DTE–TPE emitters show sub-100 nm resolution which is higher than for conventional fluorescent imaging. The spectroscopic and imaging data provides initial guidelines for the screening of molecular scale memory units with the corresponding excitation and detection wavelengths for signal readout and super-resolution imaging agents.

Introduction

Since thermally stable photochromic diarylethene was first introduced in 1988 by Irie,[1,2] many novel diarylethene molecules have been reported.[3–6] Dithienylethene (DTE) is one of the most utilised and developed diarylethene structures, owing to its outstanding properties, such as thermally-irreversible photoisomerization, excellent fatigue resistance and efficient photochromism performance in the solid state and even in the single-crystalline phase.[7,8] These features meet the technical requirements for optoelectronic devices. In this light, DTE has generated extensive interest in high-technology studies and applications such as optical memory media,[9–11] bioimaging,[12–15] single molecular fluorescence photoswitches,[11,16,17] optical transistors,[18] photoprogrammable organic light-emitting diodes[19,20] and light-driven actuators.[7,21] Recently, photoswitchable fluorophores have been described as promising fluorescent labels in super-resolution imaging which breaks the diffraction limit.[22–24] Thus, the design and synthesis of new fluorescent DTEs are vitally important in novel imaging with nanoscale resolution.

In most reports regarding luminescence as a detection or readout signal, the photochromes are investigated in solution.[25–27] However, the optoelectronic applications of photoswitches often require the photoswitch to be in the solid or aggregate state.[28] As a popular phenomenon in organic solid state luminescence, aggregation causing quenching (ACQ) in highly-loaded solid films must be overcome, even though some fluorescence systems in polymer films for optoelectronic applications have been reported.[26] Therefore, the design of photochromic systems to surmount the challenges of ACQ is required.

Within the last few years, great progress has been made regarding materials which display aggregation induced emission (AIE) properties.[29–31] The AIE materials, such as 1-methyl-1,2,3,4,5-pentaphenylsilole[32] and tetraphenylethene (TPE),[33,34] exhibit opposing properties to the more commonly observed ACQ materials, and have excellent fluorescence quantum efficiencies in the solid-state in contrast to near quenching in solution. As the most AIE-active materials besides siloles, TPE-based materials are easy to synthesise and modify, and exhibit high AIE effect values (extent of the emission enhancement) and excellent solid-state fluorescence. Because of these properties, TPE-based materials have attracted increased attention in the fields of OLEDs and chemo/biosensors. Taking advantage of the attractive properties of

[a]*Wuhan National Laboratory for Optoelectronics and College of Optoelectronic Science and Technology, 1037 Luoyu Road, Wuhan, Hubei 430074, China. E-mail: mqzhu@hust.edu.cn; leo@mail.hust.edu.cn*

[b]*College of Chemistry and Chemical Engineering, 1037 Luoyu Road, Wuhan, Hubei 430074, China*

[c]*Department of Biomedical Engineering, Huazhong University of Science and Technology, Wuhan, Hubei 430074, China*

† Electronic supplementary information (ESI) available. See DOI: 10.1039/c3ra40674a

‡ These authors contributed equally to the practical work.

TPE, it is desirable to design dithienylethene–tetraphenylethene (DTE–TPE) conjugates which enable AIE behaviour and fluorescence photoswitching. We report the synthesis and optical properties of the first TPE-based photochromic material, DTE–TPE, which quenches its fluorescence in solution and exhibits enhanced bright green luminescence when present in nanoparticles and the solid state. We investigate the AIE behaviour, photochromism and fluorescence photoswitching of the photochrome. Solid state patterns have been fabricated which exhibit ''on–off'' reversible fluorescence switching and readout capability. Particularly, the super-resolution fluorescence imaging of DTE–TPE dispersed in a polymethylmethacrylate (PMMA) matrix has been reconstructed as a nano-resolution pattern based on the photoswitchable AIE of DTE–TPE.

Results and discussion

Synthesis and charaterization

Scheme 1 shows the synthetic procedure for the open form of DTE–TPE. Chlorination of 2-methylthiophene at the 5-position was carried out smoothly, due to the relatively low chlorination reactivity at the 3-position compared with the 5-position, obtaining 2-chloro-2-methylthiophene in high yield (83%). Subsequent bromination at the 4-position by bromine in chloroform at 0 °C afforded 3-bromo-2-chloro-5-methylthiophene in excellent yield (93%). It is expected that the Cl atom at the 5-position of 3-bromo-5-chloro-2-methylthiophene is stable enough to withstand attack by butyllithium, while the bromine atom of 3-bromo-5-chloro-2-methylthiophene can undergo exclusive lithium–halogen exchange at −78 °C. The formed intermediate, 5-chloro-2-methyl-3-thienyllithium, was reacted with perfluorocyclopentene, and after purification, 1,2-bis-(5-chloro-2-methyl-3-thienyl)perfluorocyclopentene (Di-Cl-DTE) was obtained as white crystals in moderate yield (30%). Finally, Di-Cl-DTE and TPE–$B(OH)_2$[33] were easily conjugated by Suzuki cross-coupling in good yield (63.4%). The open form and photostationary state (PSS) of DTE–TPE were characterizated by ^{1}H NMR spectroscopy, mass spectrometry and HPLC.

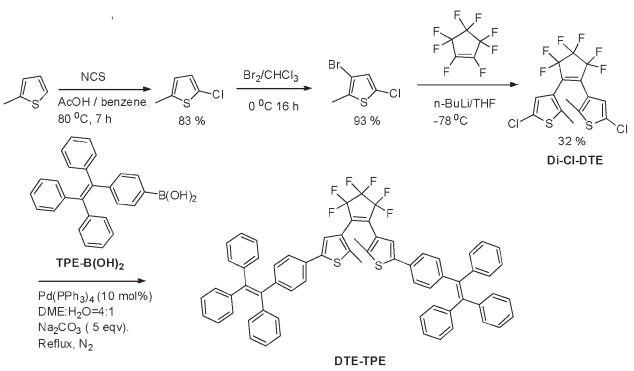

Scheme 1 (a) Synthetic procedure for DTE–TPE.

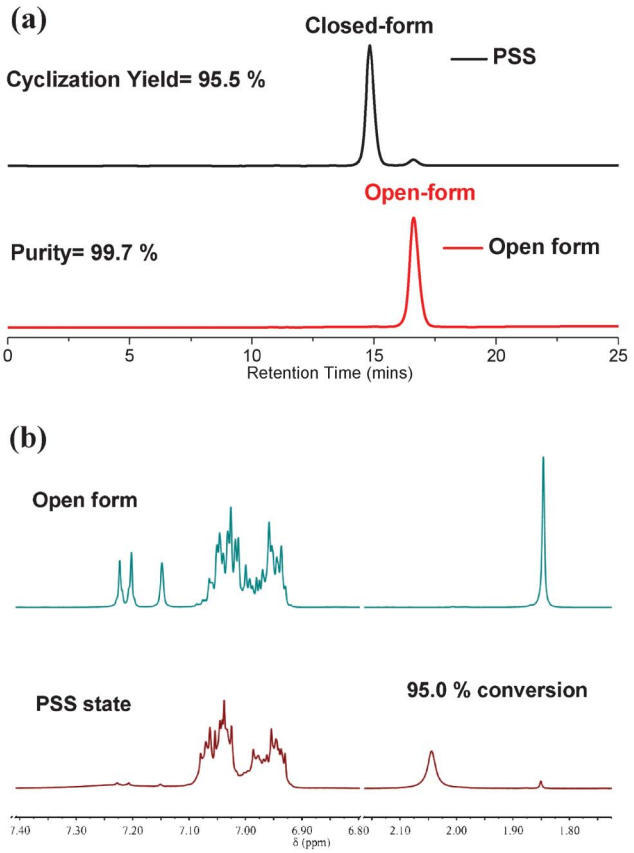

Fig. 1 Purity and isomerization yields of DTE–TPE-O and DTE–TPE-C. (a) Chromatograms of TPE–DTE in the open form and PSS. Mobile phase = 3% hexane in DCM. (b) ^{1}H NMR spectra of TPE–DTE (4 mg mL^{-1}) in the open form and PSS, after 30 min of 365 nm irradiation in CD_2Cl_2.

The detailed synthesis and characterization of DTE–TPE-O is provided in the ESI.†

The purity of DTE–TPE and the ratio of the open form (DTE–TPE-O) to the closed form (DTE–TPE-C) was obtained by HPLC. The HPLC UV detector was set at 368 nm, which is the isosbestic point of the photoswitching process of DTE–TPE. It means that the molar absorption coefficients of DTE–TPE-O and DTE–TPE-C are equal at this wavelength. Therefore, the area percentages of the peaks in the HPLC spectra represent the corresponding ''real'' molar concentration of DTE–TPE-O and DTE–TPE-C. The single peak at 16.61 min corresponds to DTE–TPE-O with a 99.7% purity of DTE–TPE (Fig. 1a). After saturated irradiation with UV light (365 nm), the PSS of DTE–TPE was achieved with a 95.5% ring-closing yield. The ^{1}H NMR results are in good agreement with the results obtained by HPLC. From the ^{1}H NMR spectra (Fig. 1b), DTE–TPE-O and DTE–TPE-C can be easily distinguished, with the chemical shift of the $-CH_3$ group on the thiophene ring of DTE–TPE-O located at 1.85 ppm, and for DTE–TPE-C the $-CH_3$ group shift is located at 2.04 ppm. The ratio of these two integrals gives a ring-closing yield of 95%.

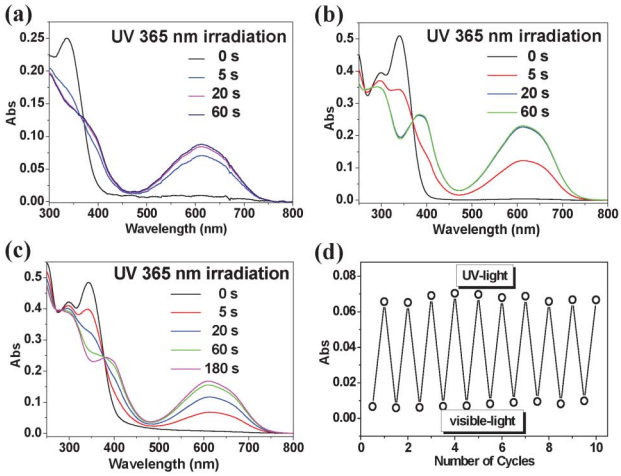

Fig. 2 Optical properties of DTE–TPE. Absorption spectra of DTE–TPE: (a) at 3 wt% in a PMMA matrix, (b) in THF (5×10^{-5} M) and (c) in water : THF 95 : 5 (v/v) (5×10^{-5} M) at different 365 nm light irradiation times. (d) Cycling behavior of DTE–TPE from the open to closed forms in the solid state, monitored at 610 nm using visible light and UV light.

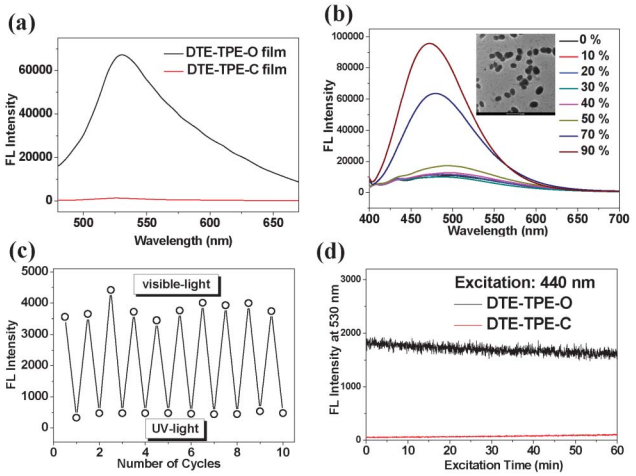

Fig. 3 Fluorescence properties of DTE–TPE: (a) fluorescence spectra of DTE–TPE-O and DTE–TPE-C in the solid state (excitation at 440 nm), (b) emission spectra of DTE–TPE in different THF–water solvent mixtures (concentration = 1×10^{-4} M, excitation at 385 nm); the inset shows the TEM image after evaporation of 90% of the water fraction, showing a nanoparticle size of ~250 nm, (c) reversible fluorescence switching of DTE–TPE in the solid state (excitation at 440 nm, emission at 530 nm) using visible light and UV light, (d) change in the fluorescence intensity (at 530 nm) of DTE–TPE-O and TPE–DTE-C in the solid state with excitation at 440 nm.

UV-vis absorption properties

Fig. 2 shows the absorption spectra of DTE–TPE upon irradiation with 365 nm light when in THF, as nanoparticles (water : THF = 95 : 5, v/v) and as a solid film. DTE–TPE underwent a photochromic reaction in THF, nanoparticles and the solid state upon irradiation with 365 nm light for 1 min. The open form, DTE–TPE-O, did not show strong absorption in the visible region above 400 nm. The absorption band in the visible region (λ_{max} = 610 nm) was assigned to the closed form, DTE–TPE-C. Upon 365 nm UV irradiation at 0.97 mW (photon flux: 2.8×10^{-9} Einstein) for 20 s, DTE–TPE in THF and in PMMA attained 98% and 96% absorbance at the 365 nm PSS (the equilibrium state under 365 nm irradiation) respectively, while DTE–TPE nanoparticles attained about 90% of the PSS upon 1 min of 365 nm irradiation, probably due to the light scattering of the DTE–TPE nanoparticles. (Fig. 2a–c). The opposing cycloreversion process takes around 3 min in THF, indicating a slightly slower process compared to the ring-closure process (Fig. S1, ESI†). This indicates that molecular chain rigidity and skeleton motion blocking in the nanoparticles slows down the photochromic reaction. The absorbance of DTE–TPE increased and decreased reversibly in solution and in the nanoparticles and PMMA films with alternating UV and visible light irradiation, demonstrating the highly reversible and bistable photochromism of DTE–TPE. (Fig. 2d) Optimized structures of both the ring-opening and ring-closing isomers of DTE–TPE *via* density functional theory (DFT) are shown in Fig. S2, ESI.† In the open form, DTE–TPE-O, the HOMO is delocalized over the entire molecule with significant orbital density on both the TPEs and the thiophene rings. Comparably, the HOMO in DTE–TPE-C is focused on the core between the thiophenes due to the strong electron-withdrawing potential of pentafluorocyclopentene. The LUMOs of DTE–TPE-O and DTE–TPE-C are focused around the pentafluorocyclopentene.

Photoswitchable aggregation-induced emission properties

In this work, DTE–TPE was selected as an ideal fluorophore because of the large Stokes shift (λ_{abs} = 340 nm, λ_{em} = 520–540 nm), as well as the strongly enhanced fluorescence in the PMMA film, which can be optically switched with a switching ratio of 40 (Fig. 3a), and in the nanoparticle state (Fig. 3b and Fig. S3, ESI†), compared with DTE–TPE in solution. The AIE behavior can be investigated using THF–water measurements, in which the PL intensity is monitored during the gradual addition of water (anti-solvent) in different amounts to a dilute THF (solvent) solution of DTE–TPE. Fig. 3b shows a gradual increase of the PL intensity as the water fraction is increased, providing clear evidence of AIE. At a high water content, nano-precipitation occurs (see Fig. 3b inset), which hinders the internal bond motions of the TPE end-groups with a subsequent enhanced emission. This is in sharp contrast to the fluorophore in pure THF, in which the internal bond motions are excessive, and non-radiative emission dominates.

The optimal excitation wavelength for fluorescence readout was screened by monitoring the change in the fluorescence intensity of the DTE–TPE-O film under continuous excitation at different wavelengths (Fig. S4, ESI†). When the DTE–TPE-O film was irradiated with a 440 nm readout light (200 μW cm^{-2}) to induce the fluorescence excitation of DTE–TPE, the strong green fluorescence of DTE–TPE-O as well as the almost quenched fluorescence of DTE–TPE-C were monitored with a fluorescence on–off switching ratio of 10 : 80 (Fig. 3c). Continuous excitation with 440 nm light caused no detectable change of intensity at 530 nm for either DTE–TPE-O or DTE–TPE-C, indicating the preservation of the bistability of DTE–TPE. After one hour of continuous excitation with a 440 nm readout light (200 μW cm^{-2}), the fluorescence intensity at 530

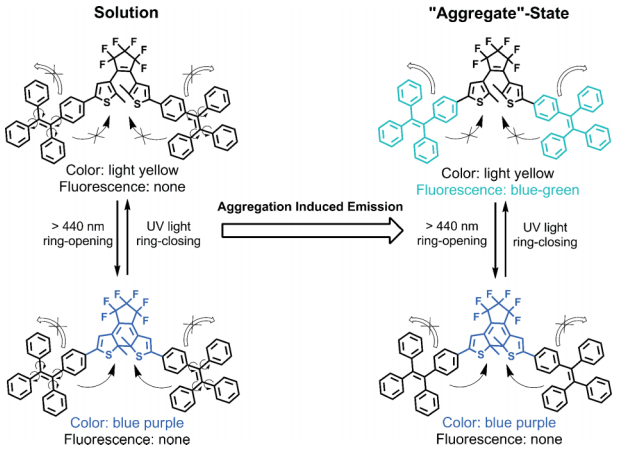

Scheme 2 Schematic of DTE–TPE-O and DTE–TPE-C showing photochromism and fluorescence/quenching in solution and the ''aggregate'' state respectively.

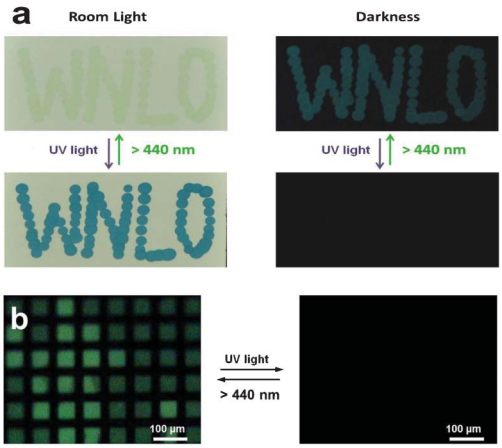

Fig. 5 Macroscopic and microscopic erasable fluorescence photoimaging. (a) Reversible photochromic (colorless to blue color, left) and fluorescent (blue-green emission to non-emission under 365 nm excitation, right) patterns. Samples prepared using a dilute DTE–TPE solution (CH_2Cl_2) and writing with a glass capillary tube on a glass TLC plate; (b) reversible fluorescent micropattern under fluorescence microscope upon visible light and UV irradiation. Excitation light: blue light (~440 nm). Samples prepared using a dilute DTE–TPE solution (CH_2Cl_2) drop-cast on a glass slide.

nm of TPE-DTE-O causes only a 7% reduction in emission intensity for DTE–TPE-O, and the increase of the quenched-state DTE–TPE-C fluorescence intensity is negligible. (Fig. 3d) This indicates that both the TPE–DTE-O and TPE–DTE-C forms are relatively photostable upon 440 nm excitation, which enables a relatively low-destructive fluorescence readout.

Scheme 2 illustrates the photochromism of DTE–TPE and the mechanisms of solution quenching and enhanced solid-state fluorescence. Non-radiative decay channels are open in solution due to excessive internal motions within the molecule, which result in quenching and non-fluorescence. In contrast, the solid state results in restriction of intramolecular rotations (RIR) of the molecules, and subsequent enhanced emission. After transformation to the closed form, the new peak at around 600 nm in the absorption spectra overlaps with the TPE emission, and energy transfer occurs which results in quenching of the emission. This process can explain the ''on-state'' and ''off-state'' phenomenon in the solid state of DTE–TPE-O and DTE–TPE-C, respectively. Photos of both of the isomeric forms in the solid state (Fig. 4) clearly show the changes in colour and fluorescence of the open and closed forms. AIE can be further confirmed by a comparison of the fluorescence quantum efficiencies (Φ_F) in solution and in PMMA using diphenylanthracene as the fluorescence standard ($\Phi_{cyclohexane}$ = 90%, Φ_{PMMA} = 83%).[34] The Φ_F is 14 times higher in PMMA (Φ = 4.2%) than in solution (Φ = 0.3%). Although the molecules are isolated in the PMMA matrix, as in solution, the rigid PMMA polymeric matrix efficiently hinders the internal rotations of the TPE end-groups, therefore enhancing the fluorescence efficiency.[33] After UV-irradiation and cyclisation to the closed form, considerable quenching is observed (Φ = 0.1%).

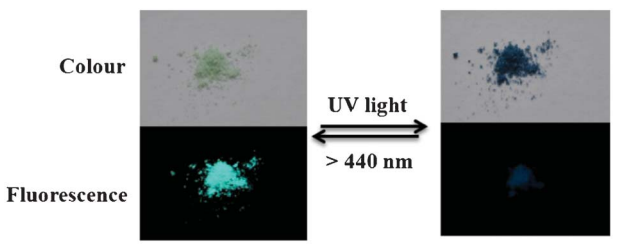

Fig. 4 Photos of the DTE–TPE-O and DTE–TPE-C powders in daylight against a white background, and under UV light (365 nm) against a black background.

Photoswitchable patterns

The strongly enhanced fluorescence of DTE–TPE-O and the quenched fluorescence of DTE–TPE-C, both of which are stable in the condensed state, produce a high and constant fluorescence on–off switching ratio, ensuring the accurate readout of information. The macroscopic and microscopic photoswitching patterns are fabricated for the demonstration of photochromism and photoswitching (Fig. 5). It is noteworthy that the colors of the pattern in the dark are a result of fluorescence. Colorless species produce blue-green emission while blue patterns under room light are non-fluorescent in the dark (Fig. 5a). The patterns are repeatedly recovered both for photochromism and fluorescence switching. By employing the patterned illumination through the square-patterned contact mask, we successfully demonstrated that the different microsized images could be effectively and reversibly recorded (>440 nm), erased (UV light), and read out (~440 nm) in the solid state (Fig. 5b). The fluorescent patterns with different colors (365 nm UV excited blue-green emission, and blue light excited green emission) are attributed to the excitation wavelength-dependent emission of DTE–TPE in the solid state. It is found that the maximum emission wavelengths depend on the excitation wavelengths (Fig. S5, ESI†). The emission peak shows a red-shift from 480 nm to 550 nm when the excitation wavelength increases from 400 nm to 480 nm. This excitation wavelength-dependent emission appears to undergo a stronger red-shift when excited at the red edge of its

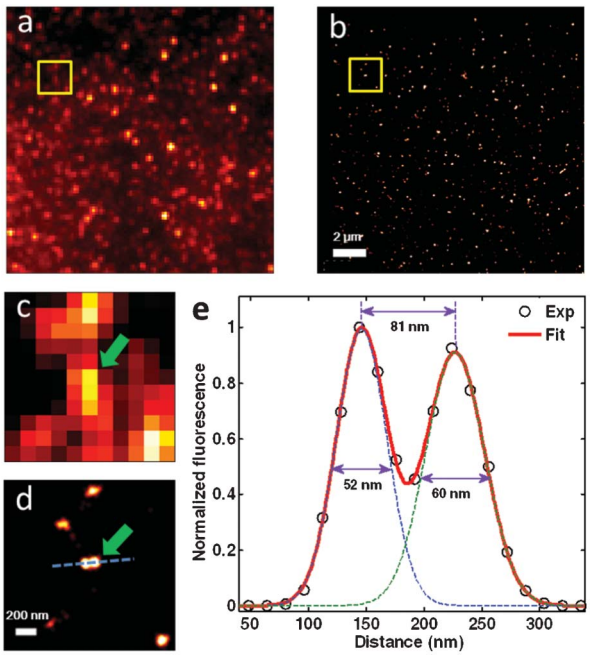

Fig. 6 Super-resolution imaging of spin-coated DTE–TPE-loaded PMMA film. (a) A conventional fluorescent image displaying the distribution of DTE–TPE fluorophores in a solid film. (b) Super-resolution fluorescent image of the same film as in (a). (c) and (d) Expanded view, and super-resolution fluorescent images, of the marked regions in (a) and (b), respectively. (e) Fluorescence cross-sectional profiles of a pair of vicinal DTE–TPE emitters along the dashed line in (d), indicating a spatial resolution of 81 nm.

absorption spectrum, which suggests a possible red-edge effect (REE),[35–37] although this hypothesis has not been verified.

Super-resolution fluorescent imaging

Through the repeated and reversible optical imaging of photoswitchable fluorophores, it is possible to reconstruct the fluorescence patterns with nanoscale resolution beyond the optical diffraction limit.[22–24,38] DTE–TPE is used as a novel super-resolution imaging agent for sub-wavelength nanostructures. Our fluorescence images are reconstructed by the high-precision localization of individual photoswitchable fluorophores which are switched on and off at different wavelength excitations. Fluorescence switching of DTE–TPE is essential in super-resolution fluorescence imaging, thus we prepared the DTE–TPE spin-coated film and inspected the imaging resolution. We distinguished the vicinal DTE–TPE emitters and their distribution in the solid film with a home-made localization-based super-resolution microscope (Fig. 6). In comparison to the conventional fluorescent image (Fig. 6a), the super-resolution image (Fig. 6b) is much clearer and makes the emitters more distinguishable. The magnified conventional fluorescent image is not of sufficient resolution to distinguish between the vicinal DTE–TPE emitters (Fig. 6c). In comparison, a much more distinct image is obtained with sub-100 nm resolution by the super-resolution imaging mode (Fig. 6d). The smallest distance between DTE–TPE emitters, which can be observed in the super-resolution image, was determined (Fig. 6e). The DTE–TPE pairs shown in Fig. 4d were measured as being 81 nm apart (Fig. 6e). The full width in half maximum (FWHM) of the two emitters was measured as about 52 nm and 60 nm, respectively. It is noteworthy that the emission intensities of the individual emitters are different, which is probably attributed to the aggregation of DTE–TPE molecules to some extent. The results indicate that DTE–TPE, as a novel super-resolution imaging agent, enables sub-100 nm fluorescence imaging.

Conclusions

In summary, we have demonstrated a novel and unique route to a highly erasable optical molecular switch which utilizes the photochromic switching of AIE-active DTE–TPE. DTE–TPE, a photochromic group, which features a large Stokes-shifted emission (180–200 nm) and solid state enhanced fluorescence, was employed as the main component of an optical molecular switch. The super-resolution fluorescence nanolocalization indicates that vicinal DTE–TPE emitters are distinguishable with sub-100 nm resolution, which is higher than in conventional fluorescent imaging. As a novel fluorescent-switchable material, the DTE–TPE conjugate has the potential for utilization in localization-based super-resolution imaging as an alternative optical nanoimaging agent.

Acknowledgements

This work was supported by the NSFC (21174045, 20874025) and the National Basic Research Program of China (2013CB922104). M. P. A. acknowledges the NSFC Research Fellowship for International Young Scientists (21150110141, 212111128) and the Special Fellowship of China Postdoctoral Science Foundation (2012T50642). M. Q. Z. acknowledges the Open Program for Beijing National Laboratory for Molecular Sciences (BNLMS) and the Fundamental Research Funds for the Central Universities (HUST2010MS101). We also thank the Analytical and Testing Center of Huazhong University of Science and Technology.

Notes and references

1 M. Irie and M. J. Mohri, *J. Org. Chem.*, 1988, **53**, 803.
2 M. Irie, *Chem. Rev.*, 2000, **100**, 1685.
3 M. Takeshita and M. Irie, *Chem. Lett.*, 1998(11), 1123.
4 A. Osuka, D. Fujikane, H. Shinmori, S. Kobatake and M. Irie, *J. Org. Chem.*, 2001, **66**, 3913.
5 H. Tian, B.-Z. Chen, H.-Y. Tu and K. Müllen, *Adv. Mater.*, 2002, **14**, 918.
6 M. Berberich and F. Würthner, *Chem. Sci.*, 2012, **3**, 2771.
7 S. Kobatake, D. Takami, H. Muto, T. Ishikawa and M. Irie, *Nature*, 2007, **446**, 778.
8 M. Morimoto and M. Irie, *Chem. Commun.*, 2005, 3895.
9 *Molecular Switches*, ed. B. L. Feringa and W. R. Browne, Wiley-VCH,Weinheim, 2nd edn, 2011.
10 S. Kawata and Y. Kawata, *Chem. Rev.*, 2000, **100**, 1777.

11 T. Fukaminato, T. Doi, N. Tamaoki, K. Okuno, Y. Ishibashi, H. Miyasaka and M. Irie, *J. Am. Chem. Soc.*, 2011, **133**, 4984.
12 Y. Zou, T. Yi, S. Xiao, F. Li, C. Li, X. Gao, J. Wu, M. Yu and C. Huang, *J. Am. Chem. Soc.*, 2008, **130**, 15750.
13 M.-Q. Zhu, G.-F. Zhang, C. Li, M. P. Aldred, E. Chang, R. A. Drezek and A. D. Q. Li, *J. Am. Chem. Soc.*, 2011, **133**, 365.
14 M.-Q. Zhu, G.-F. Zhang, C. Li, Y.-J. Li, M. P. Aldred and A. D. Q. Li, *Journal of Innovative Optical Health Sciences*, 2011, **4**, 395.
15 M.-Q. Zhu, L. Zhu, J. J. Han, W. Wu, J. K. Hurst and A. D. Q. Li, *J. Am. Chem. Soc.*, 2006, **128**, 4303.
16 M. Irie, T. Fukaminato, T. Sasaki, N. Tamai and T. Kawai, *Nature*, 2002, **420**, 759.
17 T. Fukaminato, T. Sasaki, T. Kawai, N. Tamai and M. Irie, *J. Am. Chem. Soc.*, 2004, **126**, 14843.
18 M. Pärs, C. C. Hofmann, K. Willinger, P. Bauer, M. Thelakkat and J. Köhler, *Angew. Chem., Int. Ed.*, 2011, **50**, 11405.
19 P. Zacharias, M. C. Gather, A. Köhnen, N. Rehmann and K. Meerholz, *Angew. Chem., Int. Ed.*, 2009, **48**, 4038.
20 Z. Zhang, X.-D. Liu, Z.-Y. Li, Z.-I. Chen, F.-Q. Zhao, F.-I. Zhang and C.-H. Tung, *Adv. Funct. Mater.*, 2008, **18**, 302.
21 U. Al-Atar, R. Fernandes, B. Johnse, D. Baillie and N. R. Branda, *J. Am. Chem. Soc.*, 2009, **131**, 15966.
22 M. J. Rust, M. Bates and X.-W. Zhuang, *Nat. Methods*, 2006, **3**, 793.
23 B. Huang, W. Wang, M. Bates and X.-W. Zhuang, *Science*, 2008, **319**, 810.
24 M. Bates, B. Huang, G. T. Dempsey and X.-W. Zhuang, *Science*, 2007, **317**, 1749.
25 K. Uno, H. Niikura, M. Morimoto, Y. Ishibashi, H. Miyasaka and M. Irie, *J. Am. Chem. Soc.*, 2011, **133**, 13558.
26 A. J. Myles, B. Gorodetsky and N. R. Branda, *Adv. Mater.*, 2004, **16**, 922.
27 J. Kärnbratt, M. Hammarson, S. Li, H. L. Anderson, B. Albinsson and J. Andréasson, *Angew. Chem., Int. Ed.*, 2010, **49**, 1854.
28 Q.-F. Luo, H. Cheng and H. Tian, *Polym. Chem.*, 2011, **2**, 2435.
29 Y.-N. Hong, J. W. Y. Lam and B.-Z. Tang, *Chem. Soc. Rev.*, 2011, **40**, 5361.
30 A.-J. Qin, J. W. Y. Lam and B.-Z. Tang, *Prog. Polym. Sci.*, 2012, **37**, 182.
31 Z.-J. Zhao, J. W. Y. Lam and B.-Z. Tang, *J. Mater. Chem.*, 2012, **22**, 23726.
32 J.-D. Luo, Z.-L. Xie, J. W. Y. Lam, L. Cheng, H.-Y. Chen, C.-F. Qiu, H. S. Kwok, X.-W. Zhan, Y.-Q. Liu, D. Zhu and B.-Z. Tang, *Chem. Commun.*, 2001, 1740.
33 M. P. Aldred, C. Li, G.-F. Zhang, W.-L. Gong and M.-Q. Zhu, *J. Mater. Chem.*, 2012, **22**, 7515.
34 (*a*) G.-F. Zhang, M. P. Aldred, W.-L. Gong, C. Li and M.-Q. Zhu, *Chem. Commun.*, 2012, **48**, 7711; (*b*) W.-L. Gong, F. Zhong, M. P. Aldred, Q. Fu, T. Chen, D.-K. Huang, Y. Shen, X.-F. Qiao, D.-G. Ma and M.-Q. Zhu, *RSC Adv.*, 2012, **2**, 10821; (*c*) M. P. Aldred, C. Li and M.-Q. Zhu, *Chem.–Eur. J.*, 2012, **18**, 16037.
35 A. P. Demchenko, *Luminescence*, 2002, **17**, 19.
36 A. J. Boydston, P. D. Vu, O. L. Dykhno, V. Chang, A. R. Wyatt II, A. S. Stockett, E. T. Ritschdorff, J. B. Shear and C. W. Bielawski, *J. Am. Chem. Soc.*, 2008, **130**, 3143.
37 A. Paul, P. K. Mandal and A. Samanta, *Chem. Phys. Lett.*, 2005, **402**, 375.
38 S. J. Lord, N. R. Conley, H. L. Lee, R. Samuel, N. Liu, R. J. Twieg and W. E. Moerner, *J. Am. Chem. Soc.*, 2008, **130**, 9204.

